Computational Study on the Effect of Axial Ligation Upon the Electronic Structure of Copper (II) Porphyrinate (CuTPPs = [5,10,15,20-tetrakis(N-methylpyridyl-4)porhinato]copper(II)tetratosylate)) - Electronic Structure with Different Axial Ligands

Roxana-Viruca Ţolan, Alexandru Lupan*, Radu Silaghi-Dumitrescu
Department of Chemistry, Faculty of Chemistry and Chemical Engineering,"Babes-Bolyai" University, Arany Janos Str. no. 11, RO-400028, Cluj Napoca, Romania.
alupan@chem.ubbcluj.ro*

(Received on 5th December 2013, accepted in revised form 22nd December 2015)

Summary: Copper porphyrins are generally known to show a less diverse reactivity as compared to their iron counterparts, both redox-wise and in terms of axial ligation. Reported here are density functional theory (DFT) results on models of copper (II)-porphyrins (models of [5,10,15,20-tetrakis(N-methylpyridyl-4)porhinato]copper(II)tetratosylate) with a set of axial ligands – nitrite (both the nitrogen-bound isomer and the oxygen-bound isomer, i.e., nitro and nitrito), imidazole, two forms of phenol (neutral and anionic), and water - related to an unexpected range of electronic structures detectable in electron paramagnetic resonance (EPR) spectra of a water-soluble copper porphyrin with water, nitrite, imidazole, dithionite, 2,2'-azino-bis(3-ethylbenzthiazoline-6-sulphonic acid) (ABTS) and guaiacol. Computed spin densities and atomic charges reveal various degrees of influence of the axial ligands on the Cu-porphyrin electronic structure, which may be related to the notably different changes induced by each ligand (imidazole, nitrite, guaiacol and ABTS) on the EPR superhyperfine splitting, but with an unexpectedly strong dependence on choice of the computational methodology. Thus, at the B3LYP/6-31G** level the copper spin densities are predicted to range from 0.69 to 0.73 depending on the axial ligand, this contribution being located on the d_{x2-y2} orbital in a range from 65% to 100%. BP86/DN** results tend to favor a distinctly larger spread of these values.

Keywords: copper, porphyrin, DFT, spin, EPR, molecular orbital.

Introduction

Copper porphyrins show a less diverse reactivity as compared to iron porphyrins, both redox-wise and in terms of axial ligation. Oxidation reactions of the Cu(II)-porphyrin complexes typically take place at the porphyrin ligand while the central copper ion remains in the oxidation state of +2; in contrast iron, manganese or cobalt can lead to formal oxidation states as high as +5 [1, 2].

Copper(II) porphyrins can bind to DNA due to the absence of a fifth axial ligand and are capable of both binding and intercalation exhibiting preference for GC (guanine-cytosine) base pairs [3]. However, there is little direct evidence for axial ligand exchange reactions at the copper in porphyrins. Another copper-porphyrin complex (sodium-copper chlorophyllin) has been shown to act as an inhibitor and also as a promoter of DNA-damage induction by a variety of mutagens [4].

The water-soluble copper porphyrinate, copper (II) porphyrinate (CuTPPs = [5,10,15,20-tetrakis(N-methylpyridyl-4)porhinato]copper(II) tetratosylate)), was previously examined by UV-Vis and electron paramagnetic (EPR) spectroscopy for its ability to engage in a number of reactions involving either axial ligation to the copper or possible redox cycling, with ligands and potential redox partners such as nitrite, imidazole, dithionite, 2,2'-azino-bis(3-ethylbenzthiazoline-6-sulphonic acid) (ABTS) and guaiacol [5]. Almost non-detectable changes in the UV-vis spectra of CuTPPs were noted, in contrast to an unexpected range of electronic structures clearly detectable in the EPR spectra [5]. The superhyperfine coupling seen in the CuTPPs spectra with some of the ligands was distinctly larger than anything previously reported for iron porphyrins or related systems [6], and was reminiscent of previously noted manifestations in copper porphyrinate complexes [7]. The present work aims to investigate the electronic structure basis of these changes in EPR spectra, employing theoretical methods. Indeed, computational methods, especially density functional theory and to some extent semiempirical ones, generally provide useful insight into transition metal complexes, including porphyrinates [8].

Experimental

Density functional theory (DFT) calculations were carried out using the Gaussian 09 [22], Spartan 5 [23] and Spartan '06 [24] software

*To whom all correspondence should be addressed.

packages. The Results section discusses Gaussian 09 results, unless otherwise specified.

All the structures considered in the study (Fig. 1) were constructed using the graphical interface of Spartan '06 program. Geometry optimizations and frequencies analysis were carried out using the gradient corrected hybrid density functional B3LYP [25-28] in conjugation with 6-31G** basis set in Gaussian 09 and in Spartan '06. The choice of B3LYP/6-31G** is based on the fact that it has been demonstrated that B3LYP is excellent in modeling this type of molecules [29-32]. Default convergence criteria were employed in each software package.

Single-point calculations of structures **1-7** in water were also performed using B3LYP/6-31G** on gas-phase-optimized geometries, using the COSMO model as implemented in Gaussian09 (CPCM) [33]. For molecules **1-7** a natural bond orbitals analysis (NBO) [34] was also performed in Gaussian. Ligand binding energies were calculated with formula ΔE = [E(model) - E(model 1) - E(ligand)], where E is the each model energy calculated with Spartan '06.

Results and Discussion

Reported here are computational data on copper (II) porphyrinate (CuTPPs) complexes, in the context of the previously discussed [5] unexpected range of electronic structures detectable in EPR spectra. In the experimental measurements the axial ligands were nitrite, imidazole, dithionite, ABTS and guaiacol (Fig. 1). The axial ligands employed in our calculations are therefore nitrite, imidazole, and two forms of phenol (neutral and anionic) . The latter is used as a model for guaiacol and/or ABTS. Also examined was a water ligand, since the EPR spectra were recorded in water. Modeling binding of dithionite to the copper was not attempted, due to the fact that multiple binding modes are possible not only for dithionite but also for its several possible decomposition products (e.g. SO_2^-, $S_2O_3^{2-}$, SO_3^{2-}). The optimized geometries for models **1-7** are shown in Fig. 2, with energies reported in Table-1.

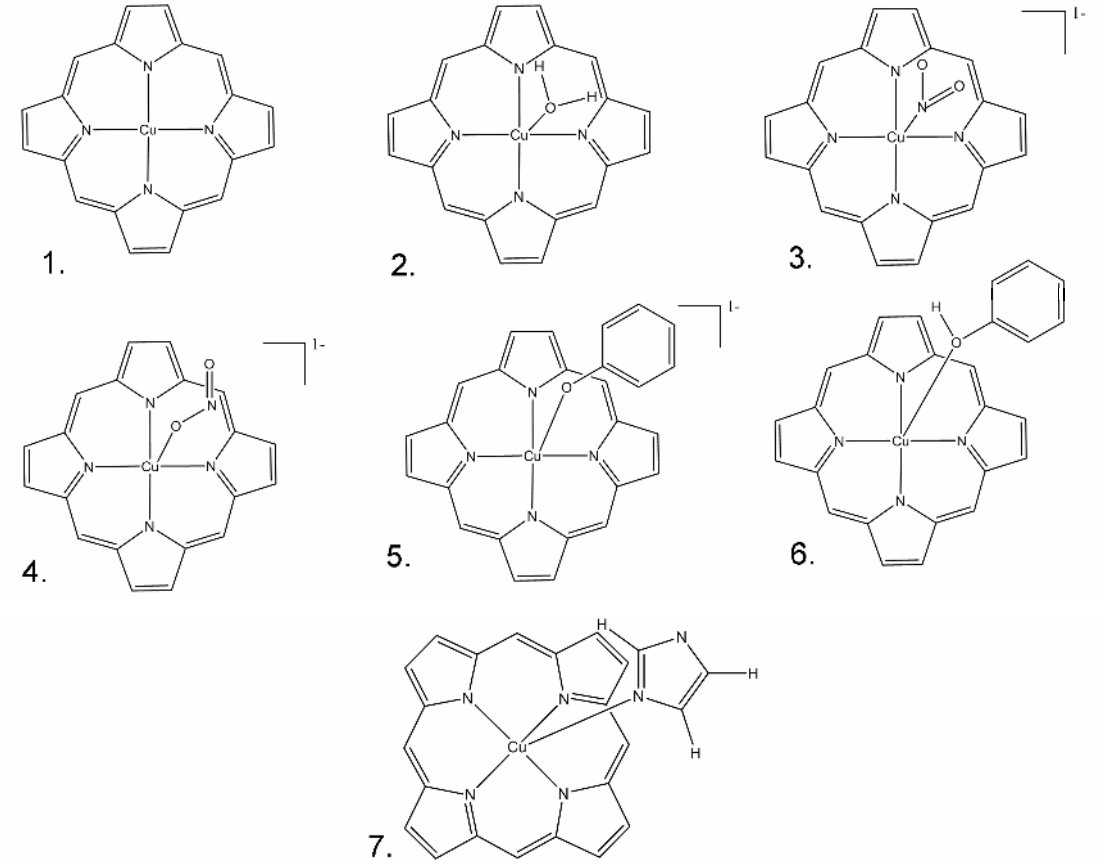

Fig. 1: Models employed in the present study.

Table-1: Calculated energy and ligand binding energies. ΔE=[E(model)-E(model 1)-E(ligand)].

No.	E (hartree)	ΔE(kcal/mol)
1	-2628.770282	0
2	-2705.200431	-6.5
3	-2833.925829	-22.0
4	-2843.930806	-25.0
5	-2935.684879	-13.9
6	-2936.256475	-4.8
7	-2855.002833	-5.7

As seen in Fig. 2, structure **1** remains entirely planar as expected. In the other structures, the copper is slightly displaced out of the porphyrin plane, depending on the strength of the axial bonds; these displacements are, however, generally very small, cf. Table-2: between 0.02 and 0.06 Å for the weakly-binding water and phenol, and between 0.22 and 0.45 Å for the more properly bound nitrite, phenolate and imidazole – with the maximum distance seen for the O-nitrite adduct. For the latter case, the distance between the metal and the plane defined by the macrocycle nitrogens is ~double compared to what is computed for a model where the Cu(II) was replaced with Fe(III) or Fe(II) (0.17 Å, cf. geometries reported in [9] and similar ones in [10, 11] – arguably because of a larger radius of the copper compared to iron (van der Waals radius of 1.57 Å compared to 1.31 Å, respectively).

In structure **2** the water ligand forms two hydrogen bonds with the nitrogen atoms from the porphyrin (N---H distances of ~2.5 Å cf. Table-2, which is shorter than the sum of van der Waals radii of nitrogen and hydrogen, of 2.75 Å). In structure **6** (the phenol adduct) the same happens with the hydrogen atom from protonated phenol, with the 2.16 Å N—H distance (cf. Table-2) indicating a hydrogen bond stronger than those established by water. The hydrogen bonds established in models **2** and **6** are paralleled by the fact that the bond lengths between Cu and O are particularly elongated; in fact, with 2.71 and 3.17 Å, these Cu-O distances are longer than the N---H hydrogen bonds and, in the case of the phenol adducts, even longer than the sum of van der Waals radii of copper and oxygen, suggesting no attractive interaction between these two atoms. This suggests that any association between water or hydroxylic ligands with Cu(II) porphyrins can be expected to mainly involve hydrogen bonding to the nitrogens, rather than direct metal-oxygen coordination. Indeed out of 242 structures identified in the Cambridge Cristallographic datatabase [12] only 7 contain Cu-O bonds; four have neutral oxygen ligands [13-16] and the Cu-O bond in these is particularly long (generally 2.5-2.7 Å) with the exception of [16] where the protons of the water ligand bound to the Cu are strongly interacting with the hexafluoroantimonate anions presumably giving water a partial anionic character and allowing it to lie within 2.2 Å of the Cu. Also, of the 242 structures only five others contain axial ligands to the Cu (one with Cl [17] and four with N [18-20]), all with bond lengths between 2.4-2.6 Å. All of these experimental data are therefore in good agreement with the calculations reported here (Table-2).

Table-3 shows the evolution of energy for models **2-7** upon elongation of the axial bond lengths by 1 Å. These values provide an estimate of the axial bond strength, since in the elongated structures the Cu-axial ligand distances are all higher than the sum of van der Waals radii. These bond strengths are larger in structures **3**, **4**, and **5,** where the ligands are anionic and the bonds are shorter (Cu-L distances of 2.18 Å, 2.11 Å, respectively 2.08 Å, cf. Table-2) compared to structures **2** and **6** (Cu-L distances of 2.71 Å respectively 3.17 Å, as the ligand-macrocycle bonds are essentially hydrogen-bonding in nature). When nitrite binds in an O-coordinate fashion to copper (structure **4**), the Cu---O bond is stronger by ~3 kcal/mol compared to Cu---N bond from N-coordinate binding mode (structure **3**), in contrast to the case of the similar iron (II) and (III) and cobalt (II) and (III) complexes, where the N-nitrite isomer was preferred [9]. The energy differences computed for models **2** and **6** (Table-3) suggest essentially identical binding energies (~2.6 kcal/mol) even though the number of hydrogen bonds between the ligand and the macrocycle differs (two with water, one with phenol). The weakness of these hydrogen bonds (~half compared to a typical strong hydrogen bond) suggests that compounds **2** and **6** are unlikely to be found as stable static structures in solution. In structure **7**, where the imidazole ligand is neutral, the Cu---N bond is relatively weak (ΔE=4.7 kcal/mol, comparable to the energy of a strong hydrogen bond); such weakness of the axial bonds, especially with imidazole or thiolate ligands, has also been noted with iron porphyrins [21].

Table-4 shows computed Mulliken atomic spin densities for models **1-7** (Fig. 3). The differences between the copper spin densities in these 7 structures are not major, as the values range from 0.67 to 0.73. The nitrogen spin density, with values between 0.083 and 0.064, is relatively small but, summed up over the four nitrogen atoms, does amount to an ~30% of the spin density being delocalized away from the copper. As expected, the orbitals with unpaired electrons are $d_{x^2-y^2}$ with lobes pointing to the four nitrogen atoms (Fig. 3). Part of the spin density is also localized in the d_{yz} orbital (structure **5**), while in structure **6** the d_{xz} and d_{z^2} orbitals are also involved (cf. Table-5).

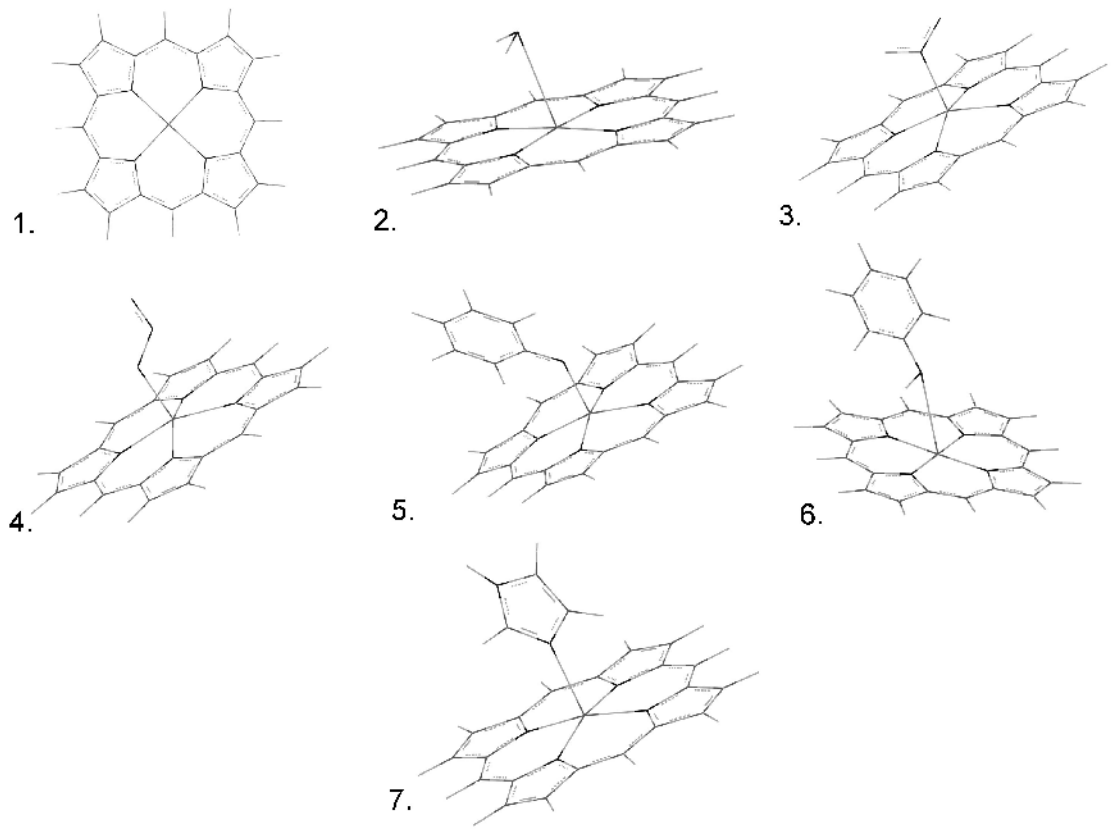

Fig. 2: Optimized geometries for models **1-7**.

Table-2: Calculated Cu-X (X=O, N), N(porphyrin)-H(ligand) and Cu-porphyrin plane (Cu-P) distances, in Å.

No.	Cu-N1	Cu-N2	Cu-N3	Cu-N4	Cu-N*	Cu-P	Cu-O	N1-H1	N2-H2	Cu-N5
1.	2.00	2.00	2.00	2.00	2.00	0.00	-	-	-	-
2.	2.02	2.02	2.00	2.00	2.01	0.06	2.71	2.48	2.51	-
3.	2.05	2.05	2.05	2.05	2.05	0.34	-	-	-	2.18
4.	2.05	2.05	2.06	2.06	2.05	0.45	2.11	-	-	-
5.	1.96	2.1	1.96	2.05	2.01	0.23	2.08	-	-	-
6.	2.02	2.00	2.00	2.00	2.00	0.02	3.17	2.16	-	-
7.	2.02	2.02	2.03	2.03	2.02	0.22	-	-	-	2.36

*average of the Cu-N bonds lengths

Table-3: Energy variation for models **2-7** upon elongation of the axial bond lengths by 1 Å.

No.	ΔE (kcal/mol)
2	2.58
3	13.3
4	16.4
5	10.6
6	2.60
7	4.70

In structures **2** and **6** the spin densities on the four nitrogen atoms are larger than for most models, except model **1** (Table-6). In these two cases there is no copper-oxygen interaction, which makes **2** and **6** very similar to **1**. Comparing structures **2** and **7** with in structure **7**, which has proper axial ligation, the interaction between copper and nitrogen from imidazole decreases the spin density on the four nitrogen atoms of the porphyrin to a value of 0.073 as compared to the 0.079 seen in structure **2**. The hydrogen bonds affect the nitrogen spin density, insofar as nitrogens involved in such hydrogen bonds tend to have somewhat less spin density; indeed, spin density in nitrogen is inversely correlated with the total charge, and a higher charge would be required for efficient hydrogen bonding.

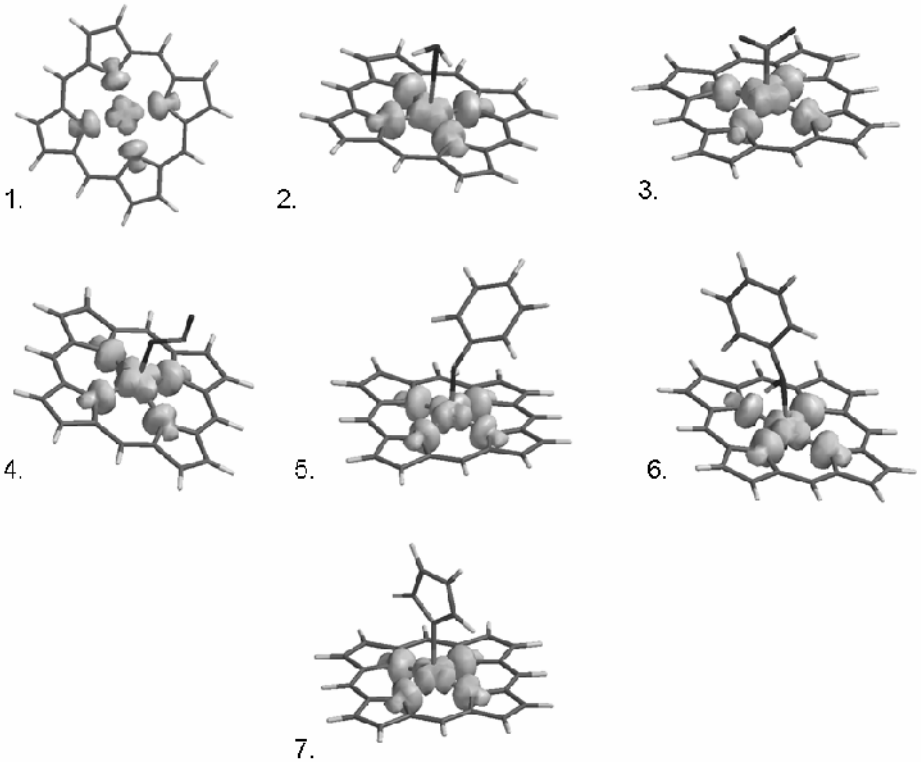

Fig. 3: Spin densities computed for models 1-7.

The influence of ligands on Cu-porphyrin electronic structure is unexpectedly small, compared to what one might have expected based on the notably different changes induced by each ligand (imidazole, nitrite, guaiacol and ABTS) on the EPR superhyperfine splitting [5]. Indeed, the copper $g_{\perp}$ signal (g=2.06) displays superhyperfine coupling from the four nitrogen atoms of the porphyrin leading to a complex pattern with peak-to-peak distance of 17 G. While this coupling is almost unobservable in the starting material (aqueous copper porphyrin), it becomes detectable with distinctly different intensities in the several spectra shown in ref. [5]. A small difference is observed in spin densities at the copper and at the porphyrin nitrogen atoms in structures **3** and **4** comparatively with structure **1**, where copper has no axial ligand. Copper spin density increases under the nitrite axial ligation influence (from 0.67 in structure **1** to 0.72 and 0.73 in structures **3** and **4**), while nitrogen spin densities decrease (from 0.080 in structure **1** to 0.067 and 0.064 – 0.066 in structures **3** and **4**) (Table-4). In the EPR spectra, the superhyperfine coupling emerges notably detectable in presence of nitrite as axial ligand [5], which is the opposite of what one would expect based on the trends of spin density on porphyrin nitrogens computed by DFT. Phenolate as copper axial ligand in structure **5** has the same effect as nitrite on copper and nitrogen spin densities, while for protonated phenol as ligand (in structure **6**), the differences are much smaller (Table-4). Comparing these results with EPR spectrum [5] of CuTPPs with guaiacol and ABTS which shows significant superhyperfine coupling, the experimental data not only indicates more considerable changes in the electronic structure than computations, but also, as in the case of nitrite as ligand, an opposite trend to what is expected based on DFT-derived nitrogen spin densities. In structure **7**, imidazole increases copper spin density (from 0.67 in structure **1**, to 0.70) and decreases spin density in porphyrin nitrogen atoms (from 0.080 in structure **1** to 0.073), while the changes induced by this ligand in the EPR superhyperfine splitting are much larger and again of opposite nature [5]. This is unexpected, and leads to the more detailed analyses reported below.

The trend in the magnitude of superhyperfine coupling effects seen in the experimental EPR spectra is (phenolic system)>imidazole>nitrite [5]. One would expect to see the same trend followed by DFT-derived spin densities. This trend can be supported if one assumes non-protonated phenol as ligand, but not if phenolate coordination is considered.

Table-4: Calculated Mulliken atomic charges and atomic spin densities for models **1-7** in vacuum. Values for the porphyrin and axial ligands are 0.00, and therefore not shown.

No.	Cu (charge)	Cu	N1	N2	N3	N4	N1+N2+N3+N4
1.	0.85	0.670	0.080	0.080	0.080	0.080	0.320
2.	0.82	0.690	0.079	0.075	0.079	0.075	0.310
3.	0.78	0.720	0.067	0.067	0.067	0.067	0.270
4.	0.76	0.730	0.064	0.066	0.064	0.066	0.260
5.	0.80	0.730	0.064	0.064	0.064	0.064	0.260
6.	0.82	0.670	0.083	0.076	0.080	0.080	0.320
7.	0.88	0.700	0.073	0.074	0.073	0.073	0.290

The copper Mulliken atomic charges for models **1-7** are shown in Table-5. Copper charges in structure **1**, where there is no axial ligand and in structure **7** have larger values, 0.85 and 0.88 respectively. In structures with anionic axial ligands, **3, 4** and **5**, copper charges are smaller, 0.78, 0.76 and 0.80, which is partly due to a different overall charge of the model in these systems. In structures **1**, **2**, **6** and **7** the copper atomic spin densities values are smaller, but the atomic charges are larger than in structures **3, 4** and **5** (Table-4).

Table-5 illustrates that in models **5** and **6** (with phenol and phenolate as axial ligands) the net spin density at the copper is partly due to contributions of two other d orbitals, leaving even less spin in the d_{x2-y2} – the orbital directly pushing spin density onto the nitrogens. This is again at odds with expectations based on the EPR spectra, where the phenol-type systems seem to have the largest amount of spin delocalization towards to porphyrin nitrogens.

Table-5: Copper d occupied orbitals (NPA analysis).

No.	d orbitals	Cu
1.	x^2-y^2	0.69
2.	x^2-y^2	0.70
3.	x^2-y^2	0.74
4.	x^2-y^2	0.74
5.	x^2-y^2	0.59
	yz	0.16
6.	xz	0.16
	x^2-y^2	0.48
	z^2	0.06
7.	x^2-y^2	0.72

Single point calculations for models **1-7** were also performed in water. The influence of solvation on Cu-porphyrin spin densities is minor, cf. Table-6. In structure **1** solvation produces no change, most likely because the molecule is symmetrical to the point where its dipole moment is zero. In the models involving neutral ligands, the computed spin densities are smaller than in vacuum, which implies, as discussed above when examining hydrogen bonding to water and phenol, an expected increase in polarization of the Cu-nitrogen bonds. In the models involving anionic ligands, the spin density values of the porphyrin nitrogen atoms increase from 0.067 in vacuum to 0.071 in water in model **3**, respectively from 0.064 to 0.068, for models **4** and **5** (Table-6), while the copper spin densities decrease.

Table-6: Calculated Mulliken atomic charges and atomic spin densities in water. Values for the porphyrin and axial ligands are 0.00, and therefore not shown.

No.	Cu (charge)	Cu	N1	N2	N3	N4	N1+N2+N3+N4
1.	0.86	0.670	0.080	0.080	0.080	0.080	0.320
2.	0.85	0.680	0.079	0.076	0.079	0.076	0.310
3.	0.83	0.700	0.071	0.071	0.071	0.071	0.280
4.	0.82	0.710	0.068	0.069	0.068	0.069	0.270
5.	0.89	0.720	0.068	0.067	0.067	0.068	0.270
6.	0.85	0.67	0.083	0.077	0.080	0.080	0.320
7.	0.93	0.67	0.073	0.074	0.073	0.073	0.290

Solvation also induces minor changes in the copper atomic charges: these decrease under the influence of water in all models, but more in structures with anionic axial ligands **3** (from 0.83 to 0.78), **4** (from 0.82 to 0.76) and **5** (from 0.89 to 0.80) (Table-6). An inverse correlation between copper Mulliken atomic spin densities and copper Mulliken atomic charges in structures **1-7** is maintained in solvent compared to vacuum (Table-6) – which, as pointed out above, is mostly due to differences in overall charges on the models. Calculations in solvent thus indicate only minor changes in Cu-porphyrin electronic structure in presence of axial ligands.

The additional structures **8-11** (Fig. 4) were also optimized, in order to verify if calculations on more realistic models can provide better agreement with the EPR spectra [5]. As seen in Fig. 5 and in Table-7, models **8** and **10** remain planar after optimization. In models **9** and **11** the copper is slightly displaced out of the porphyrin plane, with slightly longer Cu-N distances (Table-7). In general thus, the overall geometry of the macrocycle is only marginally affected by the lateral substituents.

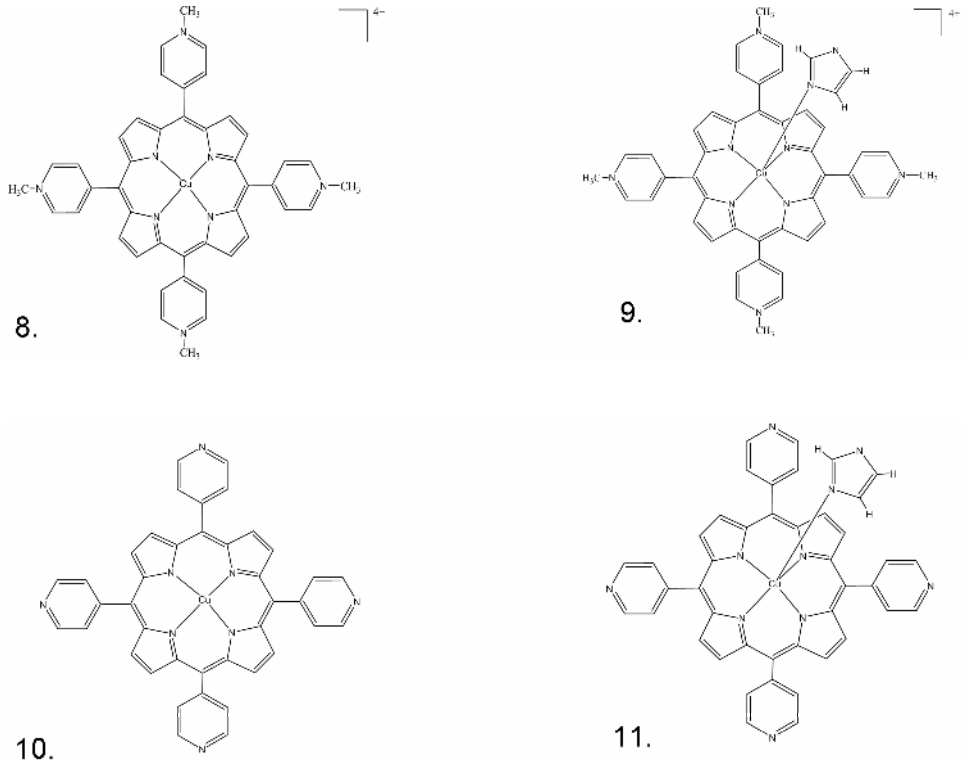

Fig. 4: Laterally-substituted models employed in present study.

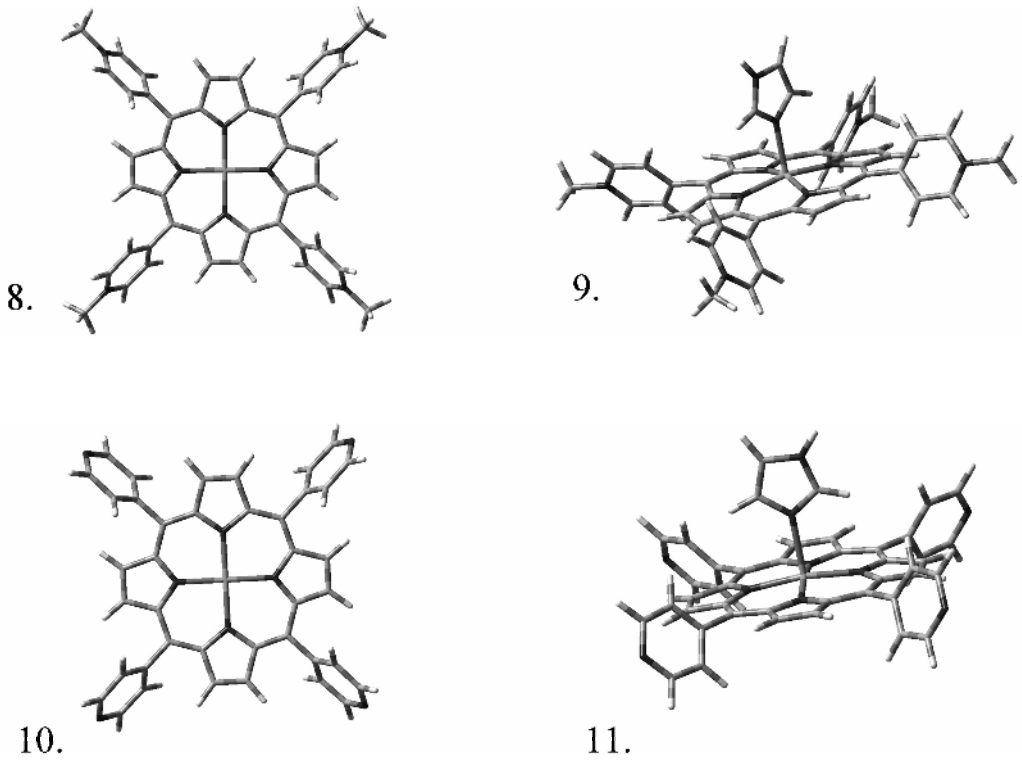

Fig. 5: Optimized geometries for models **8-11**.

Table-7: Calculated Cu-N distances (Å).

No.	Cu-N1	Cu-N2	Cu-N3	Cu-N4	Cu-N*	Cu-N5
8.	2.01	2.01	2.01	2.01	2.01	-
9.	2.04	2.05	2.04	2.05	2.04	2.28
10.	2.00	2.00	2.00	2.00	2.00	-
11.	2.03	2.03	2.03	2.03	2.03	2.35

*average of the Cu-N bonds lengths

The spin densities computed for copper and nitrogen in models **8** and **9** are similar to those in **10** and **11** (Table-8). The copper charges are larger in the methylated structures **9** and **11** (0.95 and 0.92), than in structures **8** and **10** (0.90 and 0.86) (Table-8). Comparing structures **8** with **9** and **10** with **11**, copper charges and copper spin densities increase in both cases as an effect of imidazole ligation, while the spin densities in the four porphyrinic nitrogen atoms decrease (Table-8). Nevertheless, these differences still do not appear significantly different in magnitude compared to those observed in the smaller models.

Table-8: Calculated copper Mulliken atomic charges and atomic spin densities for models **8-11** in vacuum.

No.	Cu (charge)	Cu	N1	N2	N3	N4
8.	0.90	0.670	0.079	0.079	0.079	0.079
9.	0.95	0.720	0.069	0.072	0.069	0.071
10.	0.86	0.670	0.080	0.080	0.080	0.080
11.	0.92	0.700	0.073	0.074	0.073	0.074

Single point calculation on structures **3**, **5**, **6** and **7** were also performed using a different functional (BP86) and in a different software package [10]. The results were qualitatively identical to those discussed so far. However, the same BP86 in a third software package [9] yield entirely different data. Spin densities computed for this latter case are shown in Fig. 6. Notably, in structures **3** and **5** the spin density is clearly delocalized onto the axial ligand, contrary to the results seen in the other computational packages. As seen in Table-9, the copper spin densities computed by this alternative method are distinctly smaller than those in Table-4; moreover, in structure **3** significant spin densities is delocalized on nitrogen atom from nitrite, and to some extent a similar observation can be made on structure **5**. These results in Fig. 6 may be taken to be in good agreement with the notable changes induced by each ligand (imidazole, nitrite, guaiacol and ABTS) on the EPR superhyperfine splitting [5]. This poses an unexpected paradox and underlines concerns which may be formulated with respect to population analyses based on DFT calculations in transition metal complexes – even at the qualitative level.

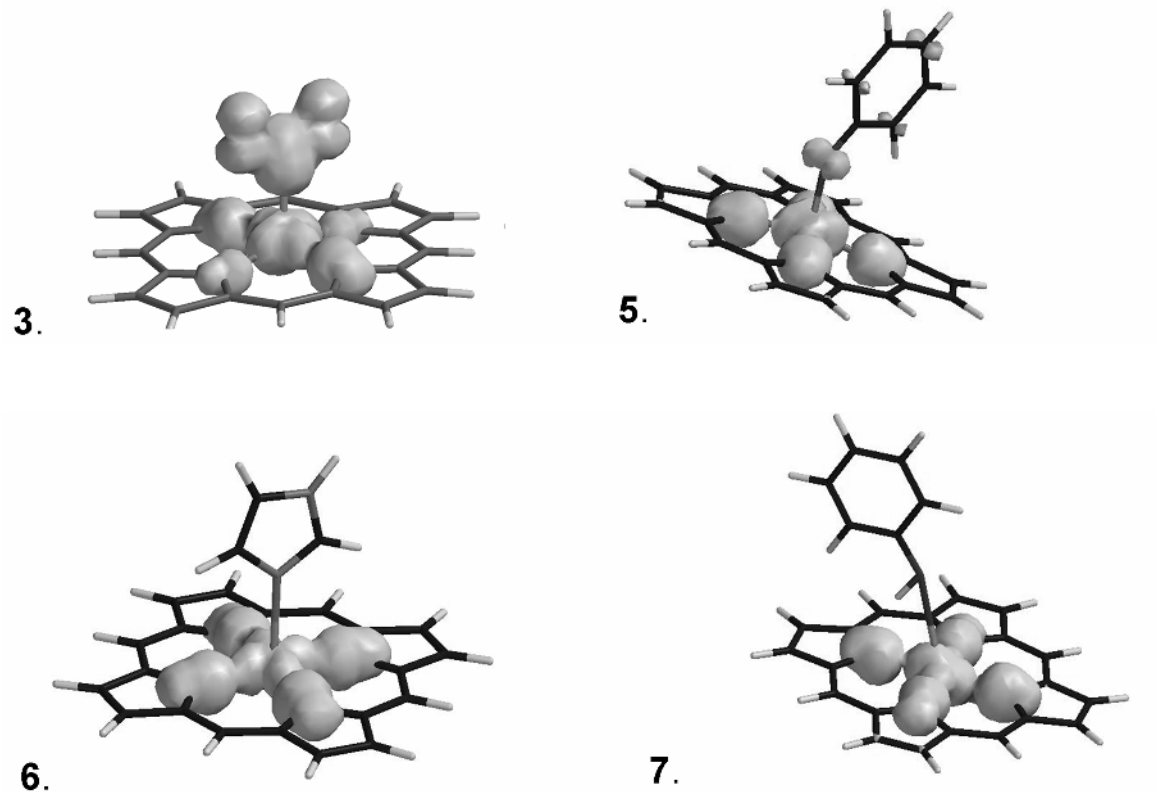

Fig. 6: Spin densities computed for structure **3**, **5**, **6** and **7** with Spartan 5.

Table-9: Calculated copper Mulliken atomic charges and atomic spin densities for models **3**, **5**, **6** and **7** with Spartan 5.

Nr.	Cu (charge)	Cu	N1	N2	N3	N4	N5	O1	O2
3.									
5.	0.55	0.510	0.066	0.075	0.074	0.065	-	0.038	-
6.	0.48	0.500	0.094	0.084	0.090	0.090	-	0	0
7.	0.50	0.520	0.086	0.087	0.087	0.087	-	-	-

Conclusion

DFT calculations using a rather standard functional and basis set indicate minor changes in Cu-porphyrin electronic structure in presence of axial ligands, while in CuTPPs EPR spectra ligands as nitrite, guaiacol and ABTS induce considerable changes on the superhyperfine coupling. However, a different computational package reveals a qualitatively different picture of the spin density delocalization, in much better agreement with experiment and posing an interesting methodological problem from the computational point of view.

Acknowledgment

The work shown here has been supported by the Romanian Ministry for Education and Research project PCCE 312/2008.

References

1. R. Silaghi Dumitrescu, High-Valent Metalloporphyrins in Hydrocarbon Activation: Metal(V)-Oxo or Metal(V)-hydroxo *New J. Chem*., **34**, 1830 (2010).
2. K. M. Kadish, K. M. Smith and R. Guillard, *The Porphyrin Handbook*, Academic Press, Vol. 9, p. 1 (2000).
3. I. Haq, J. O. Trent, B. Z. Chowdhry and T. C. Jenkins, Intercalative G-Tetraplex Stabilization of Telomeric DNA by a Cationic Porphyrin, *J. Am. Chem. Soc*., **121**, 1768 (1999).
4. E. Pimentel, M. P. Cruces and S. Zimmering, A study of the inhibition/promotion effects of sodium–copper chlorophyllin (SCC)-mediated mutagenesis in somatic cells of Drosophila, *Mutat. Res*., **722**, 52 (2011).
5. A. C. Mot, S. A. Syrbu, S. V. Makarov, G. Damian and R. Silaghi-Dumitrescu, Axial ligation in water-soluble copper porphyrinates: contrasts between EPR and UV–vis, *Inorg. Chem. Commun*., **18**, 1 (2012).
6. A. C. Mot, Z. Kis, D. A. Svistunenko, G. Damian, R. Silaghi-Dumitrescu and S. V. Makarov, 'Super-reduced' iron under physiologically-relevant conditions, *Dalton Trans*., **39**, 1464 (2010).
7. C. Calle, A. Schweiger and G. Mitrikas, Continuous-Wave and Pulse EPR Study of the Copper(II) Complex of N-Confused Tetraphenylporphyrin: Direct Observation of a σ Metal−Carbon Bond, *Inorg. Chem*., **46**, 1847 (2007).
8. J. Wang, W. Zhang and S. Wu, Binding affinities of metalloporphirins, *J. Chem. Soc. Pak.,* **30**, 256 (2008).
9. R. Silaghi-Dumitrescu, S. V. Makarov, M. M. Uta, I. A. Dereven'kov and P. A. Stuzhin, Redox non-innocence of a nitrido bridge in a methane-activating dimer of iron phthalocyanine, *New J. Chem.,* **35**, 1140 (2011).
10. A. A. Attia, A. Lupan and R. Silaghi-Dumitrescu, Spin state preference and bond formation/cleavage barriers in ferrous-dioxygen heme adducts: remarkable dependence on methodology, *RSC Adv*., **3**, 26194 (2013).
11. R. Silaghi-Dumitrescu, Redox Activation of Small Molecules at Biological Metal Centers, *Struct. Bond.*, **150**, 97 (2013).
12. Cambridge Crystallographic Database, Copyright CCDC 2013, www.ccdc.cam.ac.uk
13. A. A. Sinelshchikova, S. E. Nefedov, Y. Yu. Enakieva, Y. G. Gorbunova, A. Yu. Tsivadze, K. M. Kadish, P. Chen, A. Bessmertnykh-Lemeune, C. Stern and R. Guilard, Unusual Formation of a Stable 2D Copper Porphyrin Network, *Inorg. Chem*., **52**, 999 (2013).
14. J. Q. Wang, C. X. Ren, L. H. Weng and G. X. Jin, Porphyrin–carborane organometallic assemblies based on 1, 2-dicarba-closo-dodecaborane (12) ligands, *Chem. Commun*., 162 (2006).
15. T. Kaufmann, B. Shamsai, R. S. Lu, R. Bau and G. M. Miskelly, Separation of the Rotational Isomers of Tetrakis(N-Methyl-2-pyridiniumyl)porphyrin and the Crystal Structure of α,α,α,β-(Tetrakis(N-methyl-2-pyridiniumyl)porphyrin)copper Hexacyanoferrate, *Inorg. Chem*., **34**, 5073 (1995).
16. S. Sugawara, Y. Hirata, S. Kojima, Y. Yamamoto, E. Miyazaki, K. Takimiya, S. Matsukawa, D. Hashizume, J. Mack, N. Kobayashi, Z. Fu, K. M. Kadish, Y. M. Sung, K. S. Kim and D. Kim, Synthesis, Characterization, and Spectroscopic Analysis of Antiaromatic Benzofused Metalloporphyrins, *Chem. – Eur. J.*, **18**, 3566 (2012).

17. V. Blangy, C. Heiss, V. Khlebnikov, C. Letondor, H. Stoeckli-Evans and R. Neier, Synthesis, Structure, and Complexation Properties of Partially and Completely Reduced meso-Octamethylporphyrinogens (Calix[4]pyrroles), *Angew. Chem. Int. Ed*., **48**, 1688 (2009).
18. S. Lipstman and I. Goldberg, Versatile Molecular Recognition Features of Tetra(3-pyridyl)porphyrin in Crystal Engineering, *Cryst. Growth Des*., 10, 4596 (2010).
19. M. W. Renner, K. M. Barkigia and J. Fajer, Conformational Landscapes of Nonplanar Porphyrins: Superstructure, Ligation, Binding Pockets and Oxidation Effects in Cu(II) Porphyrins, *Inorg. Chim. Acta*, **263**, 181 (1997).
20. B. Zimmer, M. Hutin, V. Bulach, M. W. Hosseini, A. de Cian and N. Kyritsakas, Coordination polymers based on porphyrin and copper: the influence of the crystallization solvents on the dimensionality of the network, *New J. Chem*., **26**, 1532 (2002).
21. R. Silaghi-Dumitrescu, The nature of the high-valent complexes in the catalytic cycles of hemoproteins, *J. Biol. Inorg. Chem.,* **9**, 471 (2004).
22. M. J. Frisch, *et al*. Gaussian 09 Revision A.02; Gaussian, Inc., Wallingford CT (2009).
23. SPARTAN 5 Unix, Wavefunction, Inc., 18401 Von Karman Avenue Suite 370, Irvine, CA 148, 92612 U.S.A. (1999).
24. SPARTAN '06 for Windows, Wavefunction Inc., 18401 Von Karman Avenue, Suite 370 Irvine, CA 92612 USA (2006).
25. S. H. Vosko, L. Wilk and M. Nusair, Accurate spin-dependent electron liquid correlation energies for local spin density calculations: a critical analysis, *Can. J. Phys*., **58**, 1200 (1980).
26. A. D. Becke, Density-functional thermochemistry. III. The role of exact exchange, *J. Chem. Phys.,* **98**, 5648 (1993).
27. P. J. Stephens, F. J. Devlin, C. F. Chabalowsky and M. J. Frisch, Ab Initio Calculation of Vibrational Absorption and Circular Dichroism Spectra Using Density Functional Force Fields, *J. Phys. Chem.,* **98**, 11623 (1994).
28. C. Lee, W. Yang, R. G. Parr, Development of the Colle-Salvetti correlation-energy formula into a functional of the electron density, *Phys. Rev. B*, **37**, 785 (1988).
29. A. Ghosh, N-Confused Porphyrins and Singlet Carbenes: Is There a Connection? *Angew. Chem. Int. Ed.,* **34**, 1028 (1995).
30. A. Ghosh and J. Almlöf, The ultraviolet photoelectron spectrum of free-base porphyrin revisited. The performance of local density functional theory, *Chem. Phys. Lett.,* **213**, 519 (1993).
31. A. Ghosh and J. Almlöf, Structure and stability of cis-porphyrin, *J. Phys. Chem.,* **99**, 1073 (1995).
32. J. R. Reimers, T. X. Lue, M. J. Crossley and N. S. Hush, The Mechanism of Inner-Hydrogen Migration in Free Base Porphyrin: Ab Initio MP2 Calculations, *J. Am. Chem. Soc*., **117**, 2855 (1995).
33. V. Barone and M. Cossi, Quantum Calculation of Molecular Energies and Energy Gradients in Solution by a Conductor Solvent Model, *J. Phys. Chem*. A, **102**, 1995 (1998).
34. E. D. Gledening, A. E. Reed, J. A. Carpenter and F. Weinhold, NBO Version 3.1 as implemented in Gaussian 09.